Symmetric, asymmetric, and antiphase Turing patterns in a model system with two identical coupled layers

Lingfa Yang and Irving R. Epstein*
Department of Chemistry and Volen Center for Complex Systems, MS 015, Brandeis University, Waltham, Massachusetts 02454-9110, USA
(Received 23 May 2003; published 27 February 2004)

We study Turing pattern formation in a model reaction-diffusion system with two coupled identical layers. The coupling creates a pitchfork bifurcation, which unfolds the symmetric steady state via primary Turing instability, into a pair of distinct, unstable, asymmetric steady states (a-SS). The a-SS gain stability at a reverse Turing bifurcation. The multiple stabilities created by the coupling generate a corresponding multiplicity of structures, including symmetric, asymmetric, antiphase, and localized Turing patterns. Coexistence and competition of the different types of Turing patterns are studied. A one-dimensional localized structure exhibits striking curvature effects.

DOI: 10.1103/PhysRevE.69.026211 PACS number(s): 89.75.Kd, 82.40.Ck, 47.54.+r

I. INTRODUCTION

The Turing instability has been proposed theoretically as a mechanism for pattern formation in morphogenesis [1] and has been demonstrated experimentally in reaction-diffusion systems [2,3]. Classic Turing patterns, spontaneously arising due to the Turing instability, are stationary, periodic concentration patterns with an intrinsic wavelength. We have recently expanded the classic notion of Turing patterns in two aspects. First, the single wavelength selectivity was broadened to encompass two-wavelength selection, where two interacting Turing modes exhibit a spatial resonance that spontaneously gives rise to ''black-eye'' or ''white-eye'' hexagonal superlattices [4]. The other extension encompasses oscillatory Turing patterns [5], where a skeleton stationary Turing pattern is overlaid with a fine structure of propagating traveling waves.

Both of the above studies were performed on systems consisting of two coupled layers. Such structures are common in biological systems, where bilayer membranes or multilayer tissues are often found. Typically, particles undergo homogeneous diffusion within each layer, but the rate of diffusion between layers can be quite different. This difference in diffusion may play a significant role in embryonic development or biological morphogenesis [6].

Concentration gradients caused by chemical feeds arise in most experimental designs used to study pattern formation. Gradients are ubiquitous in biological environments. Turing patterns in such ramped systems have been studied in quasi-2D and 3D geometries [7,8]. Multiple layers tend to develop spontaneously because of the feeding ramps. A model consisting of two coupled layers provides a mathematically tractable way of examining some of the effects of parameter ramps. A two-layer model consisting of two linearly coupled Haken equations with different parameters in the two layers was studied by Bestehorn [9], who found mixed states or ''beans'' and triangles obtained by superposition of hexagons and stripes. Our focus here is not on these effects, however, but rather on the pure coupling effects that can arise when two *identical* layers are coupled.

In this paper, we consider a two-layer system in which species within each layer diffuse isotropically in two dimensions and move more slowly between layers due to the presence of a gap or a permeable or semipermeable membrane [5]. Reaction and (horizontal) diffusion in each (infinitesimally thin) layer generate 2D patterns, leading to a characteristic length scale, while the mass exchange between layers (vertical diffusion) provides coupling. We focus on how this coupling influences pattern formation. We find that interesting new patterns emerge only when the coupling is weaker than the planar diffusion. When the vertical and horizontal diffusion are matched (there is no gap between layers, or the intervening membrane is identical to the material of the layers), the system approaches 3D, and no new phenomena occur.

Two sets of properties control the behavior of a coupled-layer system: chemical (composition and concentrations of feed streams, kinetic parameters) and physical (diffusion rates within the layers, diffusive or other form of interlayer coupling). In this paper, we investigate a two-coupled-layer system in which the layers are identical with respect to their chemical and physical properties, i.e., all parameters are the same for both layers. There are no ramps. This choice distinguishes the present work from our earlier studies [4,5] and from Ref. [9] where coupled layers with different parameter values were investigated.

The diffusion coefficients are *uniform* within a layer and are the *same* for both layers but are *different* across layers. This configuration mimics stepwise changes in the diffusion transverse to the layers (third dimension) when the thickness of the layers and the gap between them are taken into consideration. Anisotropic and spatially varying diffusion coefficients have been studied in a general context using amplitude equations [10]. Here, we ignore the third dimension and treat the system as two close-coupled layers, which are approximated as infinitesimally thin. The diffusion across layers provides the coupling. We focus here on the role of the

*Electronic address: epstein@brandeis.edu

coupling, and demonstrate that it suffices to produce new and nontrivial phenomena.

We categorize the patterns found in this system as *symmetric* (s-) when the concentrations at all pairs of corresponding positions in the two layers are equal, as *asymmetric* (a-) when corresponding concentrations in the two layers differ, and as *antiphase* (anti-) when the spatially varying parts of the concentrations in the layers are of equal amplitude and opposite phase. We show that the coupling can induce a secondary bifurcation, in which, as the coupling is increased, a symmetric steady state (s-SS) subject to a primary Turing (symmetric Turing: s-Tu) instability is split into two distinct, unstable, asymmetric steady states (a-SS), followed by a reverse asymmetric Turing (a-Tu) bifurcation, in which the a-SS gains stability.

A localized structure (LS) is a stably coexisting combination of a region of one type of pattern embedded in another type of (background) pattern. One form of LS, with potential applications in information processing [11], consists of cavity solitons in a semiconductor microcavity, where optical spots (intensity peaks) can be written and erased on a homogeneous background of radiation. Pinned spirals [12] or antispirals [13] constitute another example of a LS, where Turing spots serve as cores that emit or receive waves. Most LSs arise in bistable systems, and we anticipate that the multistability in our coupled layer system may generate a variety of LSs.

II. MODEL AND BIFURCATIONS

We represent our two-coupled-layer system by a pair of coupled reaction-diffusion equations. We imagine that the two layers are identical and are fed with the same set of reagents:

$$\frac{\partial u_1}{\partial t} = F(u_1, v_1) + \nabla^2 u_1 + \eta(u_2 - u_1), \tag{1}$$

$$\frac{\partial v_1}{\partial t} = \sigma\{G(u_1, v_1) + d[\nabla^2 v_1 + \eta(v_2 - v_1)]\}, \tag{2}$$

$$\frac{\partial u_2}{\partial t} = F(u_2, v_2) + \nabla^2 u_2 + \eta(u_1 - u_2), \tag{3}$$

$$\frac{\partial v_2}{\partial t} = \sigma\{G(u_2, v_2) + d[\nabla^2 v_2 + \eta(v_1 - v_2)]\}, \tag{4}$$

where the kinetic terms are specified by the Lengyel-Epstein model [14,15], which describes the chlorine dioxide-iodine-malonic acid (CDIMA) reaction.

$$F(u,v) = a - u - 4\frac{uv}{1+u^2}, \tag{5}$$

$$G(u,v) = b\left(u - \frac{uv}{1+u^2}\right). \tag{6}$$

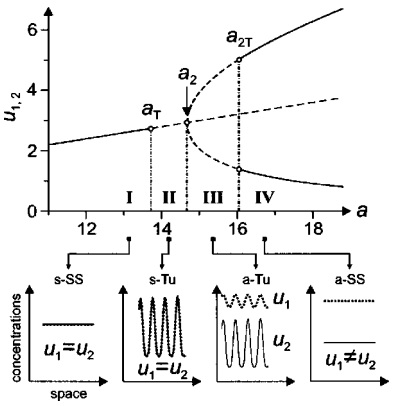

FIG. 1. Pitchfork bifurcation in the coupled layer system with $b=0.55$, $\eta=0.3$. The primary SS changes from stable (solid line) to Turing-unstable (dashed line) at the primary Turing bifurcation a_T. A pair of new SS arises at the pitchfork bifurcation a_2. They are Turing unstable (dashed lines) when born, then become stable (solid lines) at the reverse Turing bifurcation a_{2T}. Schematic solutions are shown in each of the parameter regions.

Here, u and v are the dimensionless concentrations of I^- and ClO_2^-, respectively. Concentrations in the two layers are distinguished by subscripts 1 and 2. Diffusion within each layer is described by the 2D Laplacian term, $\nabla^2 = \partial^2/\partial x^2 + \partial^2/\partial y^2$. There is a linear coupling with strength η between layers. The parameters a and b are kinetic parameters related to the feed concentrations and the rate constants; d specifies the relative mobilities of I^- and ClO_2^-, while the multiplier σ is determined by the complexing ability of the starch indicator S used in the gel [16]. We take $d=1$, $\sigma=50$ in all calculations; a or η will serve as the control parameter.

We first fix the coupling at $\eta=0.3$ and vary the chemical parameter a in order to analyze the three bifurcations (Fig. 1). At small $a<a_T$, the system has a unique stable steady state where the concentrations of the two layers are uniform and identical ($u_1=u_2=u_{SS}=a/5$). At the primary Turing bifurcation point ($a_T=13.6983$), this s-SS becomes unstable to spatial perturbations of a critical wave number $k_c=0.97$, resulting in formation of s-Tu patterns that break the spatial uniform symmetry. The concentrations of the two layers, however, remain identical ($u_1=u_2\sim e^{ik_c x}$). At a second bifurcation point, $a_2=14.6707$, a pitchfork bifurcation occurs and the concentrations of the two layers begin to diverge from one another. In this new pair of asymmetric steady states (a-SS) the concentration is higher in one layer than in the other. Turing patterns arising out of this a-SS are termed asymmetric Turing (a-Tu). By changing the coupling strength η, a_2 may approach a_T, but it never becomes smaller than a_T (Fig. 2). In this sense, the pitchfork bifurcation is a secondary bifurcation. The Turing instability ceases at $a_{2T}=16.0468$; beyond that point, the two layers are uniform in space, but have distinct concentrations in the now stable a-SS. We refer to the bifurcation at a_{2T} as a reverse Turing bifurcation because it occurs as a is varied in the opposite direction from the s-SS to s-Tu bifurcation at a_T.

The asymmetric solutions depend strongly on the coupling. If the coupling is too weak, it cannot split the s-SS

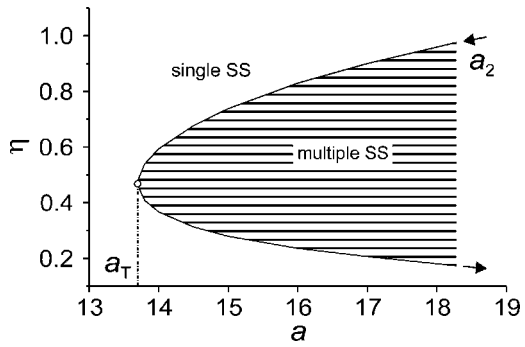

FIG. 2. Location of the pitchfork bifurcation in the $a-\eta$ plane holding $a_2 \geqslant a_T$. The bifurcation separates multiple steady states (lined area) from the single SS region.

solutions. On the other hand, with too strong a coupling the rapid exchange destroys any differences between the layers. Thus multistability can arise only in a finite range of coupling strengths. Our calculations in Fig. 3(a) show an egg-shaped region of multiple steady states.

In addition to the original primary instability, two new instabilities are induced by the coupling [Figs. 3(b)–3(e)]. At intermediate coupling levels, the two a-SS are stable, but these become unstable to Turing pattern formation toward the ends of the ''egg.'' This is the a-Tu instability, which is shown on the dispersion relations in Figs. 3(b) and 3(c). Although the concentrations in the s-SS are independent of η [horizontal dashed line in Fig. 3(a)], the stability properties of this state change as the coupling strength is varied [cf. Figs. 3(d) and 3(e)]. The original, degenerate Turing instability is split into two distinct maxima in Fig. 3(d); the left one (antiphase Turing, anti-Tu) is a coupling-dependent mode, while the right one is independent of η. As the coupling increases, the left peak in Fig. 3(d) moves to a lower wave number, flattens, and finally becomes monotonically decreasing, as shown in Fig. 3(e).

Three types of Turing instabilities: a-Tu, anti-Tu, and s-Tu, are responsible for three types of Turing pattern formation [Figs. 3(f), 3(h), and 3(j)]. (i) The a-Tu instability gives rise to an a-Tu pattern [Fig. 3(f)], where the layers have unequal concentrations that are periodic in space and stationary in time. We note that a-Tu patterns are always in-phase, the maxima and minima of one layer correspond to those of the other layer. Their occurrence and amplitude depend on η [Fig. 3(g)]. (ii) We refer to the coupling-dependent Turing mode as anti-Tu because it gives stationary Turing patterns in both layers with the same amplitude and wavelength, but opposite profiles [Fig. 3(h)]. Anti-Tu patterns occur at weak coupling, $\eta<0.65$ [Fig. 3(i)], and their amplitudes are slightly modified by η, but the average concentration remains constant at s-SS. (iii) The s-Tu patterns [Fig. 3(j)] arising from the primary Turing instability are independent of coupling strength η [Fig. 3(k)].

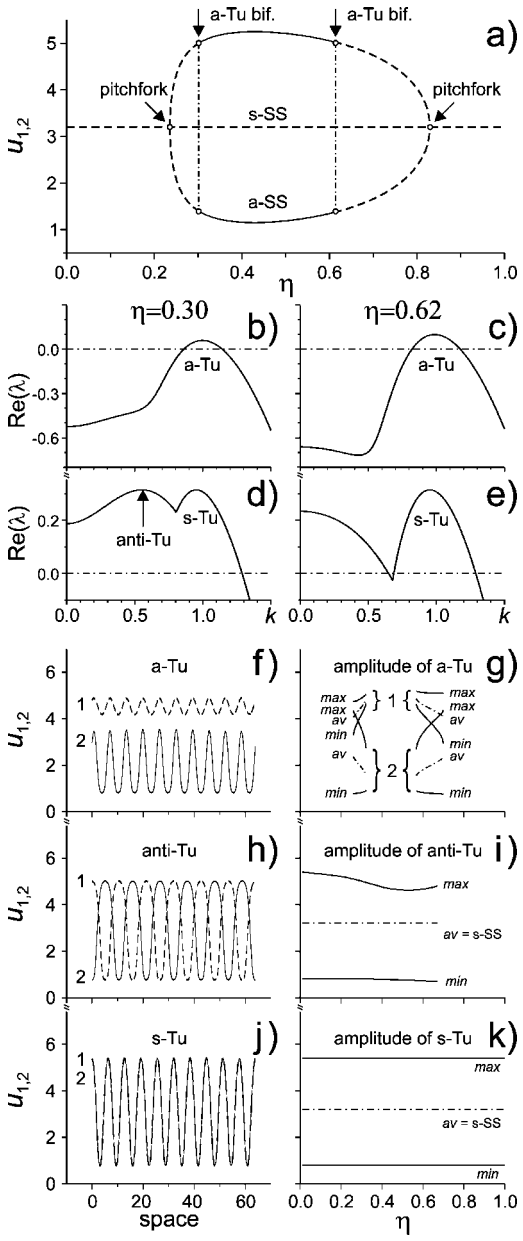

FIG. 3. (a) Bifurcation ''egg'' showing dependence of a-SS on coupling strength η for $(a,b)=(16,0.55)$. Middle sections (solid lines) are stable; two ends (dashed lines) are unstable. The central horizontal dashed line shows unstable s-SS. (b)–(e) Dispersion relations showing the most positive eigenvalue for a-SS (b),(c) and s-SS (d),(e) at $\eta=0.30$ (b),(d) and 0.62 (c),(e). Three types of Turing patterns in one-dimensional simulations, a-Tu (f), anti-Tu (h), and s-Tu (j) arise from corresponding instabilities in (b) and (d). Their occurrence (span of η) and amplitude (=max−min) are shown in (g), (i), and (k), respectively, where the average (av) is from integration over a layer.

III. COEXISTENCE AND COMPETITION OF DIFFERENT TYPES OF TURING PATTERNS

The two-dimensional (2D) Turing patterns shown in Fig. 4 all evolved spontaneously from random initial conditions with the same chemical parameters, $(a,b)=(16,0.55)$. In the single layer system, a random initial condition at $t=0$ quickly develops into a honeycomb Turing pattern at $t=40$ time units (t.u.), and then slowly decomposes into a stable stripelike pattern ($t=400$ t.u.), as shown in Fig. 4(a). In the two-coupled-layer system with coupling $\eta=0.3$, these same chemical parameters yield two different types of Turing pat-

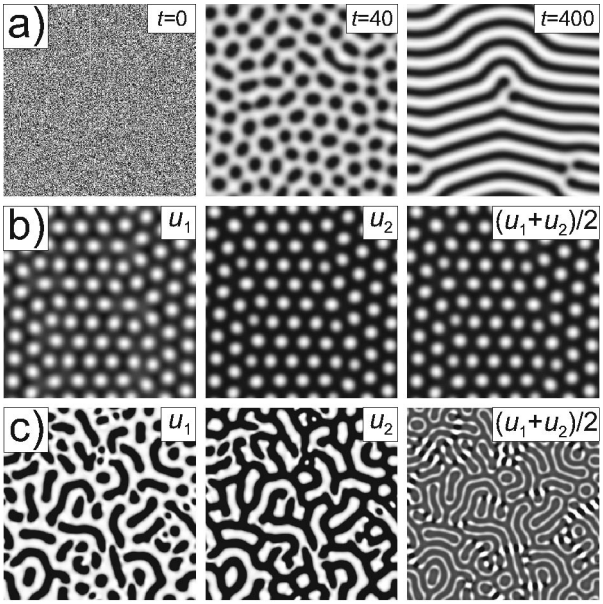

FIG. 4. Spontaneous formation of (a) stripelike Turing pattern in the single layer system, (b) spotlike a-Tu, and (c) short stripelike anti-Tu in the two-layer system. Size: 64×64 (a),(b) and 128×128 (c).

terns, depending on the initial conditions. (i) Starting from the a-SS, where the two layers have quite different concentrations, an a-Tu appears, in which the layers show an in-phase spotlike, hexagonal, stationary pattern of the same frequency [Fig. 4(b)]. (ii) Starting from the s-SS where the concentrations in the two layers are identical, an anti-Tu appears, in which both layers have a short stripelike pattern, but they are antiphase [Fig. 4(c)]. The snapshots of u_1 and u_2 look at first glance like negative images of one another.

Averaging the layers [third frames in Figs. 4(b) and 4(c)] produces frequency-doubling in the anti-Tu, while the a-Tu retains its original frequency. To explain this difference, we revisit the dispersion relations in Figs. 3(b and d), where we observe that the a-Tu instability band is narrow and close to the onset point, while the anti-Tu instability band is much broader and far above onset, which allows resonant modes to arise. The dispersion curves can also be used to predict whether the patterns will be spotlike or stripelike, since the former patterns arise immediately above onset, while stripes generally occur well beyond the onset of an instability.

The existence of two different stable patterns at the same parameters implies bistability: the a-Tu in Fig. 4(b) and the anti-Tu in Fig. 4(c) are both stable to small perturbations. With appropriate initial conditions, both structures can emerge and coexist. Figure 5 shows the coexistence of three types of Turing patterns. The system is initially prepared in an a-SS at the left and an s-SS at the right, and then small random perturbations are added as shown in Fig. 5(a). As illustrated in Figs. 4(b and c), two types of Turing patterns should, and do, develop in areas I and IV, respectively, as shown in Figs. 5(b,c,d). Close to the interface (dash-dot line section) the concentration difference on the left side constitutes a strong perturbation to the s-SS on the right side, which gives rise to anti-Tu stripes in area II followed by s-Tu

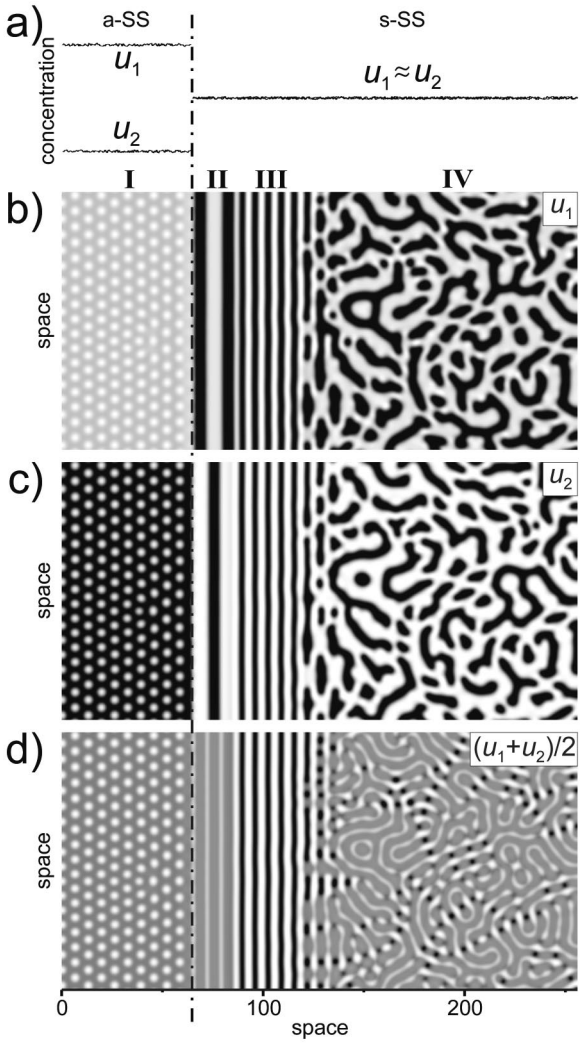

FIG. 5. Coexistence of a-, anti-, and s-Turing patterns resulting from random perturbation of initial a-SS and s-SS. (a) Initial concentrations of the two layers. (b)–(d) three views (two layers and their average) of stably coexisting patterns. System size: 128×256. Parameters as in Fig. 4.

stripes in the adjacent area III, with both stripes parallel to the interface. With this configuration, all three types of Turing patterns (a-, anti-, and s-) remain stable apparently indefinitely.

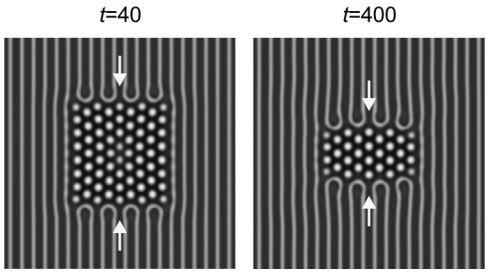

FIG. 6. Competition between a-Tu and anti-Tu shown as snapshots of $(u_1+u_2)/2$. Arrows show directions of motion of the phase border. Size 128×128, coupling $\eta=0.62$.

When more than one type of pattern is stable, competition can arise at an interface where patterns meet, and this competition can result in movement of the border or front between the patterns. The motion can be complicated due to the structure of the attractor basins in the phase plane, the border geometry, and curvature effects. A relatively simple but interesting situation involving competition between anti-Tu and a-Tu is shown in Fig. 6. The stable anti-Tu is initiated as parallel stripes with the central quarter replaced by a-SS. It then quickly develops into a-Tu ($t=40$ t.u.). The broken anti-Tu stripes approach one another along the vertical direction, swallowing the a-Tu that separates them, but they show no motion in the horizontal direction (compare snapshots at 40 and 400 t.u.). Thus the anti-Tu stripes are active at their broken ''heads'' as they overcome the a-Tu spots, but the two patterns coexist peacefully where the boundary between them is vertical.

The multiplicity of spots and stripes in a-, s-, or anti-Turing patterns in this two-layer system arises from a different source than the coexistence of spots and stripes in the single layer system. In the two-layer system, the spotlike a-Tu originates from the a-SS and the stripelike s-Tu and anti-Tu emerge from the s-SS. In the one layer system there is a region of bistability of spot- and stripelike Turing patterns, but both originate from a single monostable SS. Stability or competition in the first case depends mainly on the basins of attraction of the steady states, while in the second case it depends on the secondary instabilities of each pattern. We will show that localization in the coupled system depends on multistability, while in the single layer system localization arises from subcriticality [12].

IV. LOCALIZATION

Localization arises when different types of patterns or steady states can coexist with a stationary border separating them, and a region of one is embedded in a region of the other(s). Multistability provides the possibility of a number of localized structures in the two-layer system. On closer examination of the anti-Tu [area IV, $(u_1+u_2)/2$ snapshot] in Fig. 5(d), we note the occurrence of black dots and white ''bridges'' that form a series of dashed lines. Along these lines, the concentrations of the two layers are in-phase, rather than antiphase. These lines are localized Turing patterns, in which an s-Tu pattern is embedded in a background of anti-Tu. This lower-dimensional Turing pattern occurs along the lines of the anti-Tu phase switching.

Multistability among the three types of Turing patterns, s-, a-, and anti-, or the two types of steady states, s- and a-SS, provides numerous possibilities for different types of localized structures, which merit further study. Figure 7 shows one example, where the background is a matrix of hexagonally arranged spots (a-Tu). When this two-layer medium is locally ''burnt'' or ''written upon,'' i.e., the concentrations are reset to s-Tu at the dark spot, one bit of information is ''saved.'' Of course, the bit is erasable (by restoring the concentrations to the levels of the uniform a-Tu), like a CD-RW. Even more appealing is the medium's ''auto-correction'' feature, if the location of one bit is written incorrectly so that it

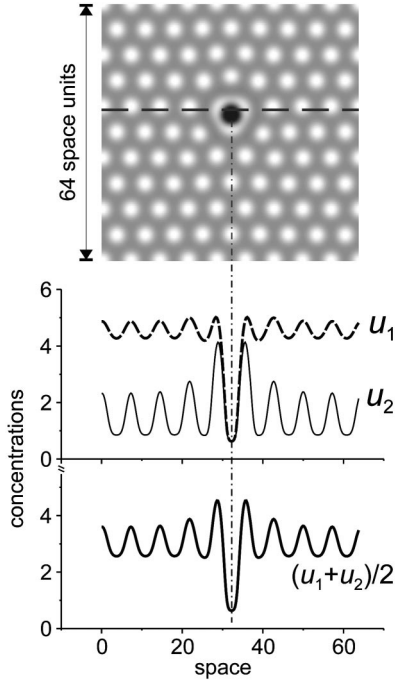

FIG. 7. Example of a stable localized structure: a single s-Tu spot is embedded in a hexagonal a-Tu lattice (top panel). The concentrations of the two layers and their average along the dashed line cut are shown in the lower panels.

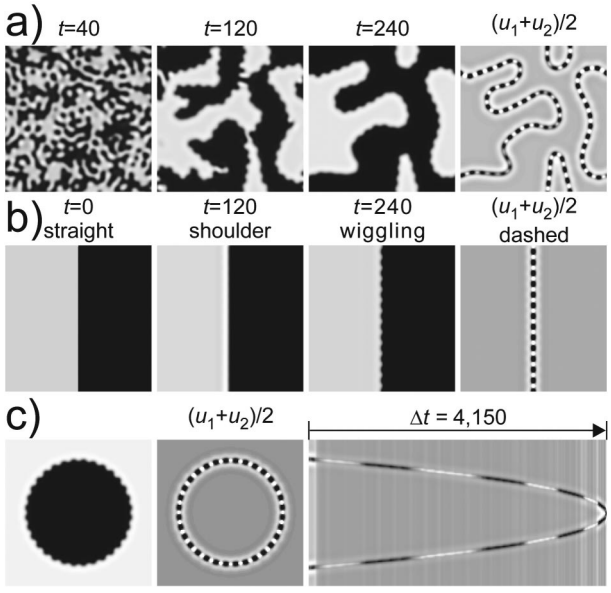

FIG. 8. Spontaneous formation of localized one-dimensional s-Tu structures at the border between antiphase clusters. $(a,b)=(12,0.2)$, $\eta=0.3$, size: 128×128. (a) Formation of antiphase clusters from random initial conditions. 1D s-Tu pattern [dashed line in plot of $(u_1+u_2)/2$] survives at phase boundary and drifts due to curvature effect. (b) Formation of s-Tu at an initially straight antiphase border. (c) Curvature effect causes shrinkage, and ultimate disappearance, of the inner phase. Rightmost panel is a space-time plot along a line through the center of the circle. Temporal behavior shows accelerating speed as curvature increases.

does not fit the matrix exactly, that bit will be pushed back into its proper position by the Turing wavelength selectivity.

Finally, an unprecedented type of localized structure arises as a result of the multistability between the a-SS patterns and the s-Tu pattern. This type of multistability occurs for $a > a_{2T}$ in Fig. 1, or for values of η in the middle part of the ''egg'' in Fig. 3(a). Starting from random initial conditions, antiphase clusters appear as shown in Fig. 8(a). The borders between the domains are rough, and the bumps on them persist as the clusters evolve. Plotting the average concentration shows that (u_1+u_2) is essentially constant everywhere except on these borders, where the concentration profile looks like a dashed line. Measuring the wavelength along this border and comparing the concentrations of u_1 and u_2, we recognize that this boundary constitutes a 1D s-Tu structure. In Fig. 8(b), we focus on the spontaneous formation of this structure by initializing the left and the right halves as two a-SS of opposite phases with a straight border between them, with cylinder boundary conditions (top connects to bottom, left and right are zero-flux). The sharp concentration profile across the border first becomes smooth and then forms a ''shoulder'' region of high concentration. Next, bumps in the average concentration begin to form along the border, ultimately becoming a dashed line like that seen in Fig. 8(a). This structure remains stable and stationary. For these kinetic parameters, the phenomenon occurs within the coupling range $0.28 < \eta < 0.42$; at weaker coupling strength, the border remains straight; with stronger coupling, s-Tu stripes grow perpendicular to the border.

The evolution of the shape of the domain boundaries in Fig. 8(a) is due to a curvature effect. To elucidate this phenomenon, we carry out the simulation shown in Fig. 8(c), where the central disk and the outer region are initialized as opposite a-SS. A dashed circle quickly forms, and then begins to shrink. The space-time plot in the rightmost frame of Fig. 8(c) demonstrates that the speed at which the border contracts is proportional to its curvature, $1/r$.

V. CONCLUSION

We have analyzed a relatively simple model consisting of two identical coupled layers. The coupling induces new bifurcations, leading to multistability. Two types of steady states, s- and a-SS, and three types, s-, a-, and anti-, of Turing patterns are obtained. Their coexistence or competition, as well as the associated phase boundary movements, merit further study. A novel one-dimensional localized structure has been found and investigated with respect to its formation and the effects of curvature. More localized structures are expected due to the multistability. Our results have been demonstrated in, but are not limited to, the Lengyel-Epstein model of the CIMA reaction. Similar coupling added to other models that possess a Turing instability should produce analogous results. The present coupled scheme should be applicable to pattern formation in morphogenesis, and the localized structures offer promise for information storage.

ACKNOWLEDGMENTS

This work was supported by the Chemistry Division of the National Science Foundation. We thank Anatol Zhabotinsky and Milos Dolnik for helpful comments.

[1] A.M. Turing, Philos. Trans. R. Soc. London, Ser. B **237**, 37 (1952).
[2] V. Castets, E. Dulos, J. Boissonade, and P. De Kepper, Phys. Rev. Lett. **64**, 2953 (1990).
[3] Q. Ouyang and H.L. Swinney, Nature (London) **352**, 610 (1991).
[4] L.F. Yang, M. Dolnik, A.M. Zhabotinsky, and I.R. Epstein, Phys. Rev. Lett. **88**, 208303 (2002).
[5] L.F. Yang and I.R. Epstein, Phys. Rev. Lett. **90**, 178303 (2003).
[6] A.V. Spirov, Int. J. Bifurcation Chaos Appl. Sci. Eng. **8**, 991 (1998).
[7] E. Dulos, P. Davies, B. Rudovics, and P. DeKepper, Physica D **98**, 53 (1996).
[8] P. Borckmans, G. Dewel, A. DeWit, and D. Walgraef, in *Chemical Waves and Patterns*, edited by R. Kapral and K. Showalter (Kluwer, Dordrecht, 1995), p. 323.
[9] M. Bestehorn, Phys. Rev. E **53**, 4842 (1996).
[10] D.L. Benson, P.K. Maini, and J.A. Sherratt, J. Math. Biol. **37**, 381 (1998); D.L. Benson, J.A. Sherratt, and P.K. Maini, Bull. Math. Biol. **55**, 365 (1993).
[11] S. Barland *et al.*, Nature (London) **419**, 699 (2002).
[12] O. Jensen, V.O. Pannbacker, E. Mosekilde, G. Dewel, and P. Borckmans, Phys. Rev. E **50**, 736 (1994); P. DeKepper, J.-J. Perraud, B. Rudovics, and E. Dulos, Int. J. Bifurcation Chaos Appl. Sci. Eng. **4**, 1215 (1994).
[13] L.F. Yang, M. Dolnik, A.M. Zhabotinsky, and I.R. Epstein, J. Chem. Phys. **117**, 7259 (2002).
[14] I. Lengyel and I.R. Epstein, Science **251**, 650 (1991); J. Phys. Chem. **96**, 7032 (1992).
[15] M. Dolnik, A.M. Zhabotinsky, and I.R. Epstein, Phys. Rev. E **63**, 026101 (2001).
[16] Relations between dimensionless parameters and concentrations of chemical species: $a = k_{1a}[\mathrm{MA}][\mathrm{I_2}]/\sqrt{\alpha}k_2[\mathrm{ClO_2}](k_{1b} + [\mathrm{I_2}])$, $b = k_{3b}[\mathrm{I_2}]/\sqrt{\alpha}k_2[\mathrm{ClO_2}]$, $d = D_{\mathrm{ClO_2^-}}/D_{\mathrm{I^-}}$, and $\sigma = 1 + (k_4/k_{-4})[\mathrm{S}][\mathrm{I_2}]$.